

# Gold-vapor-assisted chemical vapor deposition of aligned monolayer WSe<sub>2</sub> with large domain size and fast growth rate

Mingrui Chen<sup>§</sup>, Anyi Zhang<sup>§</sup>, Yihang Liu, Dingzhou Cui, Zhen Li, Yu-Han Chung, Sai Praneetha Mutyala, Matthew Mecklenburg, Xiao Nie, Chi Xu, Fanqi Wu, Qingzhou Liu, and Chongwu Zhou (✉)

Mork Family Department of Chemical Engineering and Materials Science, Ming Hsieh Department of Electrical Engineering, Core Center of Excellence in Nano Imaging and Department of Physics and Astronomy, University of Southern California, Los Angeles, CA 90089, USA

<sup>§</sup>Mingrui Chen and Anyi Zhang contributed equally to this work.

© Tsinghua University Press and Springer-Verlag GmbH Germany, part of Springer Nature 2020

Received: 21 November 2019 / Revised: 17 May 2020 / Accepted: 21 May 2020

## ABSTRACT

Orientation-controlled growth of two-dimensional (2D) transition metal dichalcogenides (TMDCs) may enable many new electronic and optical applications. However, previous studies reporting aligned growth of WSe<sub>2</sub> usually yielded very small domain sizes. Herein, we introduced gold vapor into the chemical vapor deposition (CVD) process as a catalyst to assist the growth of WSe<sub>2</sub> and successfully achieved highly aligned monolayer WSe<sub>2</sub> triangular flakes grown on *c*-plane sapphire with large domain sizes (130 μm) and fast growth rate (4.3 μm·s<sup>-1</sup>). When the aligned WSe<sub>2</sub> domains merged together, a continuous monolayer WSe<sub>2</sub> was formed with good uniformity. After transferring to Si/SiO<sub>2</sub> substrates, field effect transistors were fabricated on the continuous monolayer WSe<sub>2</sub>, and an average mobility of 12 cm<sup>2</sup>·V<sup>-1</sup>·s<sup>-1</sup> was achieved, demonstrating the good quality of the material. This report paves the way to study the effect of catalytic metal vapor in the CVD process of TMDCs and contributes a novel approach to realize the growth of aligned TMDC flakes.

## KEYWORDS

two-dimensional materials, transition metal dichalcogenides, tungsten diselenide (WSe<sub>2</sub>), chemical vapor deposition, aligned growth

## 1 Introduction

Two-dimensional (2D) layered materials beyond graphene, especially transition metal dichalcogenides (TMDCs), have attracted a lot of attention in recent years due to their intriguing properties [1, 2]. For example, tungsten diselenide (WSe<sub>2</sub>), which is one of the well-studied species among the large family of TMDCs, has been demonstrated to be a promising candidate for various applications including field-effect transistors [3–6], sensors [7, 8], and printed and flexible electronics [9–12]. Compared with the mechanical exfoliation method, chemical vapor deposition (CVD) is a better solution to achieve large-scale, good-uniformity, and high-yield TMDCs [13–16].

The orientation of TMDCs synthesized by the traditional CVD method is usually random with small size [13, 17–28]. When the growth conditions are precisely controlled, TMDC flakes can merge together to form a continuous film [17, 29]. If the orientation of the TMDC flakes is random, the grain boundaries between two flakes can significantly degrade the electronic properties of the obtained film, and thus the wafer-scale electronic applications of TMDCs could be greatly limited. However, when flakes in the same orientation merge together, seamless coalescence may lead to single-crystalline films [29, 30]. Therefore, TMDC flakes grown in the same orientation are highly preferred. In addition, aligned growth of TMDCs with large domain size is highly desired, because large flake size can reduce the formation of grain boundaries

in subsequent coalescence.

In order to achieve aligned growth of TMDCs, the selection of growth substrate is very important. Since thermally grown SiO<sub>2</sub> is amorphous, it is not suitable for aligned growth of TMDCs. As a result, many researchers have explored various substrates such as BN [18], GaN [19, 20], mica [21], graphene [22–24], and graphite [25]. The deposited TMDC domains can be aligned by the substrate lattice or step edges. Recently, *c*-plane sapphire has been widely studied as a substrate to grow aligned TMDC flakes. Dumcenco et al. achieved aligned growth of MoS<sub>2</sub> on sapphire substrates and obtained continuous films by coalescence of MoS<sub>2</sub> flakes [26], which was a significant accomplishment. However, in their work, only ~ 91.5% of the MoS<sub>2</sub> flakes are well aligned, and the relatively small flake size (~ 20 μm) and slow growth rate (~ 0.04 μm·s<sup>-1</sup>) are still limitations of their MoS<sub>2</sub> growth. Furthermore, it is known that WSe<sub>2</sub> is more challenging to synthesize than MoS<sub>2</sub>, because selenium precursor is less reactive than sulfur. In addition, WO<sub>3</sub> precursor is more difficult to sublime than MoO<sub>3</sub> (boiling points of WO<sub>3</sub> and MoO<sub>3</sub> are 1,700 and 1,155 °C, respectively), and therefore it is more difficult to control the tungsten supply than the molybdenum supply during the CVD process. Previously, we found that the WSe<sub>2</sub> flakes with a trapezoid shape can nucleate along the sapphire step edges and grow in an aligned fashion when a high-temperature treatment was applied for the *c*-plane sapphire substrates, but the typical grain size was less than 10 μm [27]. It was reported

Address correspondence to [chongwuz@usc.edu](mailto:chongwuz@usc.edu)

that atomic step-terrace structures can be formed on the surface of *c*-plane sapphire after high temperature ( $> 950\text{ }^{\circ}\text{C}$ ) annealing due to high-temperature-triggered surface reconstruction [31, 32]. Besides, some other researchers also demonstrated that aligned growth of TMDC flakes in triangle shapes is also possible using traditional CVD or metalorganic CVD on sapphire without the high temperature ( $> 950\text{ }^{\circ}\text{C}$ ) treatment, owing to the lattice match between *c*-plane sapphire and TMDCs. Huang et al. reported aligned growth of  $\text{WSe}_2$  on sapphire and the average domain size for the aligned  $\text{WSe}_2$  was about  $5\text{ }\mu\text{m}$  [13]. Eichfeld et al. [23] and Zhang et al. [17] used metal-organic CVD to achieve aligned  $\text{WSe}_2$  on sapphire, but their domain sizes were less than  $2\text{ }\mu\text{m}$  and the flakes were not strictly monolayer. In the work mentioned above, large randomly oriented  $\text{WSe}_2$  flakes up to  $100\text{ }\mu\text{m}$  can be synthesized; however, the reported flake size is much smaller when the aligned growth was achieved. There are still several problems with the state-of-art TMDC aligned growth techniques: (1) the domain size is usually very small ( $< 10\text{ }\mu\text{m}$ ) due to high nucleation density; (2) the thickness is not uniform in some reports, which would limit the electronic applications because TMDC flakes with different thickness have different bandgaps; (3) the growth rate is usually low ( $< 2\text{ }\mu\text{m}\cdot\text{min}^{-1}$ ).

By introducing Au vapor in  $\text{WSe}_2$  CVD and using *c*-plane sapphire as substrates, we have successfully achieved highly aligned monolayer  $\text{WSe}_2$  with large domain size ( $\sim 100\text{ }\mu\text{m}$ ), uniform thickness (monolayer), and fast growth rate ( $\sim 200\text{ }\mu\text{m}\cdot\text{min}^{-1}$ ). At the edge of the sapphire substrate, aligned  $\text{WSe}_2$  can also merge together to form a continuous monolayer  $\text{WSe}_2$  film. The high quality and good uniformity of the  $\text{WSe}_2$  film were confirmed using Raman spectroscopy, photoluminescence (PL), and transmission electron microscopy (TEM) characterizations. In addition, field-effect transistors (FETs) fabricated on continuous monolayer  $\text{WSe}_2$  showed good performance, indicating the potential for practical applications.

## 2 Experimental

### 2.1 Gold assisted CVD growth of $\text{WSe}_2$ on sapphire

The gold-vapor-assisted CVD process was performed in a horizontal quartz tube. The system set up is schematically illustrated in Fig. 1(a), and a photograph of the setup before the CVD process is shown in Fig. S1 in the Electronic Supplementary Material (ESM). In a typical CVD process, a piece of Au foil with  $0.1\text{ g}$   $\text{WO}_3$  was placed in a quartz boat (Boat A) and a piece of *c*-plane sapphire ( $\sim 2\text{ cm} \times 1\text{ cm}$  in size) was placed on top of the  $\text{WO}_3$  powder with the polished side facing  $\text{WO}_3$ , the position of  $\text{WO}_3$  powder is right below the upstream edge of the substrate. The vertical distance between the sapphire substrate and the gold foil is  $3\text{ mm}$ . The whole quartz boat was put in the center of the tube furnace, where the highest temperature could be achieved. Another quartz boat (Boat B) with  $1\text{ g}$  Se powders was placed upstream outside the heating zone of the furnace initially, with a stainless-steel rod used to control the position of the quartz boat during the heating process. The whole system was first evacuated to  $450\text{ Torr}$  with a vacuum pump, and then  $100\text{ sccm}$  Ar was introduced to the system as the carrier gas. Later on, the center of the furnace was gradually heated from room temperature to  $900\text{ }^{\circ}\text{C}$  in  $15\text{ min}$  and maintained at the temperature for another  $2\text{ min}$  to ensure sufficient amount of Au vapor was present in the chamber and the substrate was preheated to the desired temperature. It's worth mentioning that there was still no Se vapor in the chamber at this time since Boat B with Se powder was still outside the heating zone. Then a magnet was

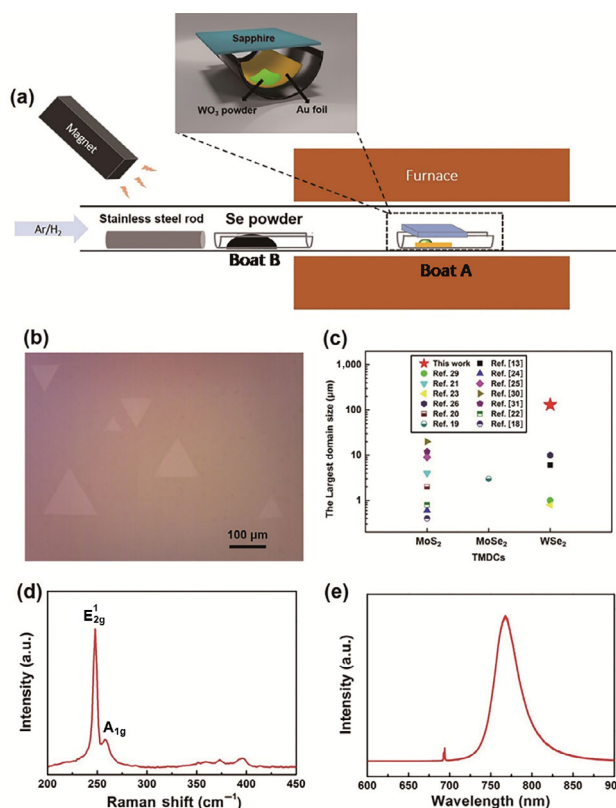


**Figure 1** (a) Schematic diagram showing the gold-vapor-assisted CVD set up. (b) An OM image showing the aligned  $\text{WSe}_2$  flakes with large domain size we can achieve. (c) Comparison study of the largest domain size between this work and previously reported aligned TMDC growth works. (d) Raman and (e) PL spectra of a typical  $\text{WSe}_2$  flake grown by the gold-vapor-assisted CVD on a sapphire substrate.

used to control the stainless-steel rod from outside the quartz tube and to push Boat B to the region with a temperature about  $250\text{ }^{\circ}\text{C}$  inside the heat zone. At the same time,  $4\text{ sccm}$   $\text{H}_2$  was introduced into the chamber to reduce the  $\text{WO}_3$  to  $\text{WO}_{3-x}$ . In this way, the chamber was filled by Se vapor and  $\text{WO}_{3-x}$  vapor to start the deposition of  $\text{WSe}_2$ . After  $30\text{ s}$  growth time, the reaction was terminated by moving both boats quickly to the low-temperature zone. Using this method, we are able to synthesize aligned monolayer  $\text{WSe}_2$  with large domain size ( $> 100\text{ }\mu\text{m}$ ) and fast growth rate ( $\sim 200\text{ }\mu\text{m}\cdot\text{min}^{-1}$ ).

### 2.2 Transfer of $\text{WSe}_2$

To fabricate field-effect transistors on as-grown  $\text{WSe}_2$  and perform TEM characterization, a modified transfer process was developed. First, the sapphire substrate with grown  $\text{WSe}_2$  was spin-coated ( $3,500\text{ rpm}$ ,  $60\text{ s}$ , baking at  $90\text{ }^{\circ}\text{C}$  for  $15\text{ min}$ ) with polystyrene (PS) solution, which was prepared by dissolving  $0.9\text{ g}$  PS ( $280,000\text{ g}\cdot\text{mol}^{-1}$ ) in  $10\text{ mL}$  toluene. Then, we scratched the PS film from the edge and immersed the substrate in hot water ( $80\text{ }^{\circ}\text{C}$ ) for  $20\text{ min}$ . Water could penetrate between the PS layer and sapphire, delaminating the PS film together with  $\text{WSe}_2$  from the substrate. The  $\text{WSe}_2$ -PS assembly was picked up by a target substrate. Subsequently, the substrate was baked at  $80\text{ }^{\circ}\text{C}$  for  $1\text{ h}$  and  $150\text{ }^{\circ}\text{C}$  for  $30\text{ min}$  to remove any water residue and eliminate possible wrinkles. Finally, the PS layer was removed by rinsing with toluene.

### 2.3 Characterizations

Raman and PL spectra were measured using a Renishaw Raman system, with  $532\text{ nm}$  laser. The TEM characterization was conducted on a JEOL JEM-2100F at  $200\text{ kV}$ . Back-gated  $\text{WSe}_2$

field-effect transistors were fabricated on Si/SiO<sub>2</sub> substrates with 285 nm SiO<sub>2</sub> following standard photolithography, development and e-beam evaporation of Ti/Au (1 nm/50 nm) source/drain electrodes. An Agilent 4156B Semiconductor Parameter Analyzer was used to measure device performance.

### 3 Result and discussion

A typical optical microscope (OM) image of WSe<sub>2</sub> flakes grown using the gold-vapor-assisted CVD approach is shown in Fig. 1(b). All the flakes have only two orientations (0° and 60°) and their thickness is uniform judging from the optical microscope image. In addition, the domain size can be larger than 100 μm. In Fig. 1(c), we compared the largest domain size in our work with other aligned TMDC work [13, 17–28]. Among all of the aligned TMDC growth work, our domain size is 4 times larger than the previous record, which reported MoS<sub>2</sub> slightly smaller than 20 μm [18–22, 24–26, 28]. More specifically, among all of the aligned WSe<sub>2</sub> growth work, our domain size is 9 times larger than the largest domain size reported previously [13, 17, 23, 27].

Raman and PL spectroscopy were collected to characterize the WSe<sub>2</sub> grown using our gold-vapor-assisted CVD. The Raman spectrum excited by a 532 nm laser is shown in Fig. 1(d). The two characteristic peaks at 248 and 259 cm<sup>-1</sup> can be attributed to E<sub>12g</sub> mode and A<sub>1g</sub> mode, respectively, indicating that the WSe<sub>2</sub> is monolayer [33]. In addition, the two high-energy peaks at 360 and 375 cm<sup>-1</sup> can be assigned to 2E<sub>1g</sub> and A<sub>1g</sub>+LA modes, but no B<sub>12g</sub> peak at ~ 307 cm<sup>-1</sup> can be observed, consistent with typical Raman spectra of monolayer WSe<sub>2</sub> [13]. The PL spectrum shown in Fig. 1(e) was also excited using a 532 nm laser. A single strong peak can be observed at 767 nm and the full width at half-maximum (FWHM) is about 34 nm. The sharp peak can be attributed to the direct bandgap emission, which is another evidence of the monolayer nature of the synthesized WSe<sub>2</sub> [34, 35].

We also found that the WSe<sub>2</sub> growth behavior had location dependence. The optical microscope images together with a statistical morphology study of WSe<sub>2</sub> flakes grown in the downstream region (defined as ~ 1 cm region from the downstream edge of the substrate) and the upstream region (defined as ~ 1 cm region from the upstream edge) on the same sapphire substrate are shown in Fig. 2. In the downstream region (Fig. 2(a)), the WSe<sub>2</sub> flakes were strictly monolayer. The edge orientation of the flakes was dominated by 0° and 60° with a ratio as high as 97%, as illustrated in the statistical analysis in Fig. 2(b). The largest flake size we observed was about 130 μm and the average size was up to 95 μm, and the corresponding size distribution is depicted in Fig. 2(c). In this way, the average growth rate in this region was as high as 3.2 μm·s<sup>-1</sup> due to the catalytic effect of Au. In comparison, the morphology of WSe<sub>2</sub> flakes grown in the upstream region of the same sapphire substrate is shown in Fig. 2(d). Obviously, the upstream region showed inferior alignment behavior and smaller domain sizes than the downstream region. Aligned behavior and 0° and 60° edge orientations were found in most of the flakes (~ 63%), as shown in Fig. 2(e). The edge sizes of the WSe<sub>2</sub> domains were usually less than 60 μm with an average size of about 37 μm, which was much smaller than the size of WSe<sub>2</sub> flakes in the downstream region. The detailed distribution of edge sizes in the upstream region is shown in Fig. 2(f). Since the Se precursor was not in the hot zone of the furnace until the starting point of the growth, we can assume that the Se vapor supply was sufficient with a constant rate. When the Se supply is limited, the WSe<sub>2</sub> flakes usually have hexagonal

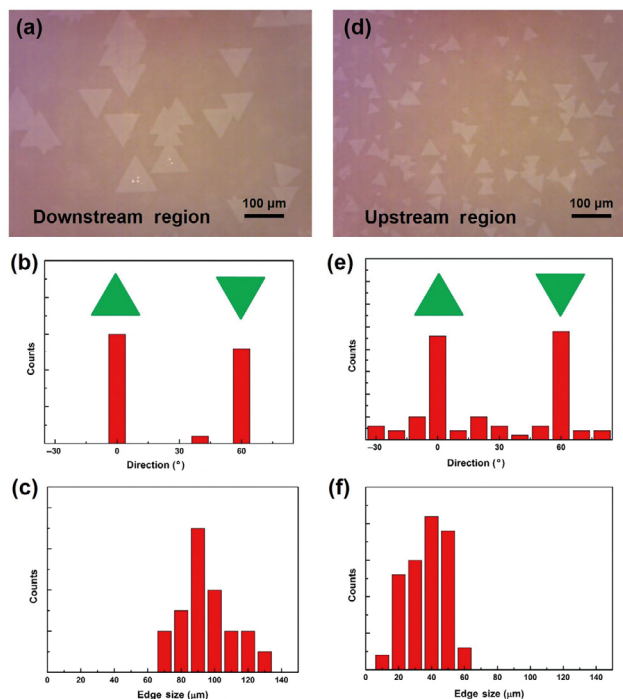


**Figure 2** (a) The OM image of the WSe<sub>2</sub> flakes grown in the downstream region, and the corresponding histograms of (b) the orientation distribution and (c) edge size distribution. (d) The OM image of the WSe<sub>2</sub> flakes grown in the upstream region, and the corresponding histograms of (e) the orientation distribution and (f) edge size distribution.

morphology. However, the WSe<sub>2</sub> flakes grown by our method are always in triangle shape, suggesting that Se supply is excess. Aljarb et al. also reported that the alignment of MoS<sub>2</sub> had location dependency, and the downstream region behaved better than the upstream region [28]. We hypothesize that this phenomenon should be highly related to the Se and WO<sub>3-x</sub> concentration in the gas phase. In the upstream region, the WO<sub>3-x</sub> concentration was higher because WO<sub>3</sub> precursor was placed right below the upstream end of the substrate. Due to the high WO<sub>3-x</sub> concentration, the growth of WSe<sub>2</sub> is under kinetic control and it was easier for WO<sub>3-x</sub> to nucleate on the sapphire substrate to form WSe<sub>2</sub> seeds. In this way, WSe<sub>2</sub> flakes are not always formed in low energy lattice matching orientation, leading to inferior alignment behavior in upstream region. In contrast, the WO<sub>3-x</sub> concentration in the downstream region was lower, the growth is under thermodynamic control, so that only WSe<sub>2</sub> seeds with good lattice matching with the substrate can be formed. Therefore, the WSe<sub>2</sub> flakes only showed 0° and 60° orientations and the incoming precursors preferred to contribute to the lateral growth of the existing flakes, resulting in larger domain size and lower nucleation density.

In order to understand the role of gold foil in the CVD process, we performed a series of control experiments following the same growth procedure but without using a gold foil. The results of control experiments with the 30-second and 5-minute growth times are shown in Fig. S2 in the ESM. When no gold foil was used, with 30 seconds growth time, which is the typical growth time we used for our gold-vapor-assisted CVD, only small nucleation seeds and small but thick WSe<sub>2</sub> flakes (~ 1 μm in size) could be found on the substrate (Fig. S1(a) in the ESM), and no large monolayer WSe<sub>2</sub> flake was observed, in contrast to Fig. 1(b). When the growth time increased to 5 min, we were able to observe WSe<sub>2</sub> monolayer flakes with thick nucleation seeds at the centers of the monolayer flakes (Fig. S1(b) in the ESM). The domain size of the monolayer flakes was around

10  $\mu\text{m}$ , and an irregular polygon grew from a single nucleation seed because it was difficult for nucleation to happen in lack of gold vapor. In addition, in our typical gold-vapor-assisted growth, the vertical distance between the sapphire substrate and the gold foil is 3 mm. We observed that when the gap distance was increased to 5 mm, thicker and smaller  $\text{WSe}_2$  flakes were obtained, because less Au vapor could reach the substrate. If the distance was further increased to 10 mm, we obtained  $\text{WSe}_2$  flakes with size and thickness similar to  $\text{WSe}_2$  flakes obtained without Au foil. This also demonstrates the key role of gold foil in the CVD process: only thick, small and randomly orientated flakes can be obtained if there is inadequate Au vapor reaching the substrate. Based on the above facts, we can confirm that the gold vapor can not only improve the growth rate dramatically, but also increase the size of obtained  $\text{WSe}_2$  flakes.

The catalytic effect of metals was reported in several previous papers, albeit with different experimental settings and results [36–44]. For example, Gao et al. used gold foils as substrates for  $\text{WS}_2$  [42] and  $\text{WSe}_2$  [43] synthesis and observed millimeter-sized domains. Due to the catalytic effect on the Au foil surface, the attachment of W and Se on the edges of  $\text{WSe}_2$  flakes is highly preferred. In addition, Liu et al. also reported that Cu vapor can assist  $\text{WSe}_2$  CVD to prepare strictly monolayer  $\text{WSe}_2$  with a fast growth rate [44]. However, neither of the above work showed orientation control. In our gold-vapor-assisted CVD system, the vapor pressure of Au is about  $5 \times 10^{-5}$  Pa, and the calculation is shown in the ESM. It's reasonable to suggest that the vaporized Au atoms tend to attach onto the edges of  $\text{WSe}_2$ , because of the high activity W and Se atoms with dangling bonds on the edges. Then, these Au atoms perform as active sites for subsequent lateral growth, which can accelerate the rate of growth and reduce the probability of nucleation and vertical growth. In combination with a lattice-matching substrate like sapphire, well-aligned  $\text{WSe}_2$  with large size can be achieved. After the growth, XPS and EDX were used to examine the Au residue on the surface of the substrate. As shown in Figs. S4 and S5 in the ESM, no discernible gold signal was detected. This is because only a trace amount of Au could be vaporized and then participated in the growth process. To demonstrate the existence of gold vapor in the system, we prolonged the growth time to 48 h while keeping all the other conditions unchanged. After 48 h, it was clear that the gold foil became tattered and gold signal was detected on the substrate through EDS (as shown in Fig. S6 in the ESM).

It's also worth mentioning that the aligned monolayer  $\text{WSe}_2$  flakes can merge to form a millimeter-sized continuous monolayer  $\text{WSe}_2$  film at locations close to the downstream edge of the sapphire substrates. The continuous  $\text{WSe}_2$  film size is typically about  $0.5 \text{ cm} \times 1 \text{ cm}$ . Figure 3(a) shows the optical microscope image of a typical continuous monolayer  $\text{WSe}_2$  region. Due to the uniformity of the  $\text{WSe}_2$  film. Figure 3(a) just shows a uniform image without any discernable pattern. The reason why continuous films are more likely to be formed close to edges of the sapphire substrate can be attributed to the higher gold vapor concentration at the edges, as the edges of the sapphire substrate are located very close to the gold foil. The Raman and PL spectra of a typical location in the continuous region is shown in Figs. 3(b) and 3(c), which are very similar to the Raman and PL of  $\text{WSe}_2$  single flakes. In the photoluminescence spectrum shown in Fig. 3(c), the single strong peak at 763 nm shows a FWHM of about 32 nm (marked in Fig. 3(c)), demonstrating the monolayer nature of the obtained continuous film. In order to confirm the uniformity, we performed Raman characterization in 5 selected positions (labeled as "a" to "e" in Fig. 3(a)), and the corresponding Raman

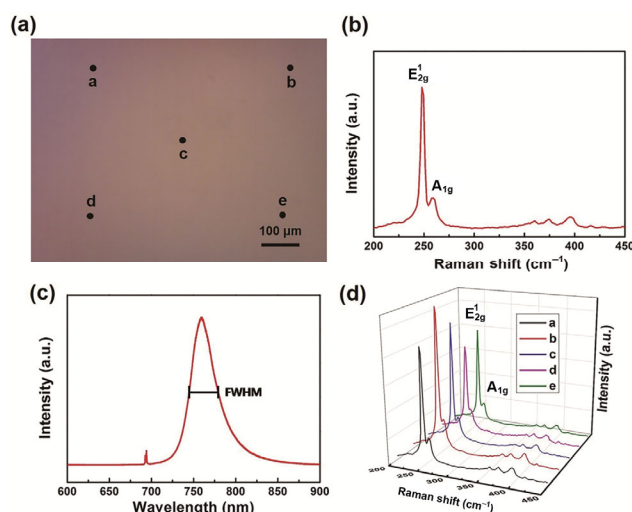


**Figure 3** (a) An OM image of a continuous monolayer  $\text{WSe}_2$  region. (b) Raman and (c) PL spectra of a typical position in the continuous region. (d) Raman spectra in the five locations a–e in (a).

spectra are exhibited in Fig. 3(d). All the Raman spectra collected in the 5 positions had strong  $E'_{2g}$  and  $A_{1g}$  peaks and no  $B'_{2g}$  peak, indicating that the aligned monolayer  $\text{WSe}_2$  flakes can merge to form a continuous monolayer  $\text{WSe}_2$  film with good uniformity. It's also worth mentioning that we observed the intermediate state of the merging process in some locations. In Fig. S3 in the ESM, the brighter part is a continuous monolayer  $\text{WSe}_2$  area, and the darker part is the exposed sapphire substrate which has not been covered by  $\text{WSe}_2$  yet. We can clearly see that most of the edges of the  $\text{WSe}_2$  are parallel to each other, indicating the perfect alignment of the  $\text{WSe}_2$  flakes before they merged together. Because of the pre-aligned lattice orientation of the individual  $\text{WSe}_2$  domains, in principle, there should be much fewer grain boundaries than a continuous film formed by  $\text{WSe}_2$  domains with random orientations [29, 30]. The reduction of grain boundary can effectively improve the electronic performance of the continuous  $\text{WSe}_2$  and is very important for large-scale electronic device fabrication.

In our CVD method, the Au foil can be repeatedly used without any extra treatment. Gao et al. used Au foil under similar conditions as our CVD growth, observed that Au foil didn't show any apparent change after being reused for 100 times [43]. Furthermore, by combining wafer-scale Au foil and more precise control of selenium and tungsten precursor supply (e.g., by using gaseous precursors), our gold assisted CVD growth with fast growth rate has potential for scalable production of  $\text{WSe}_2$ .

In order to further evaluate the quality of the  $\text{WSe}_2$  grown by our method, TEM experiments were conducted. Figure 4(a) shows a low-magnification TEM image of the straight edge of a monolayer  $\text{WSe}_2$  flake. The edge was slightly folded due to the transfer process. The selected area electron diffraction (SAED) pattern shown in Fig. 4(b) was collected in the area shown in Fig. 4(a). The SAED pattern presents only one set of six-fold symmetry diffraction spots, indicating that the as-grown  $\text{WSe}_2$  flake in Fig. 4(a) is single crystalline and has a hexagonal lattice structure. Indices of the diffraction spots are labeled in Fig. 4(b). Furthermore, the high-resolution TEM image of our monolayer  $\text{WSe}_2$  is shown in Fig. 4(c), with (100) and (110) crystal planes highlighted. The periodic honeycomb-like structure represents the atomic structure of the single crystalline  $\text{WSe}_2$ . The measured lattice distances of the (100) and (110) plane are 0.28 and 0.31 nm, which are very close

to the ideal value (shown below), only 6 and 24 pm off, respectively.

$$\frac{\sqrt{3}}{2}a_{\text{WSe}_2} = 0.2855$$

In principle, the high quality of WSe<sub>2</sub> grown by our method can lead to excellent electronic device performance. In order to explore the potential electronics applications of our aligned WSe<sub>2</sub>, we modified a wet transfer method reported in Ref. [45] to transfer our continuous monolayer WSe<sub>2</sub> to Si/SiO<sub>2</sub> substrates with 285 nm SiO<sub>2</sub> dielectric. Then, FETs were fabricated on the continuous WSe<sub>2</sub> film using photolithography followed by metal evaporation to deposit 1 nm Ti and 50 nm Au as electrodes (as shown in Fig. S7 in the ESM). The transfer characteristic of a typical back-gated FET is depicted in Fig. 5(a),

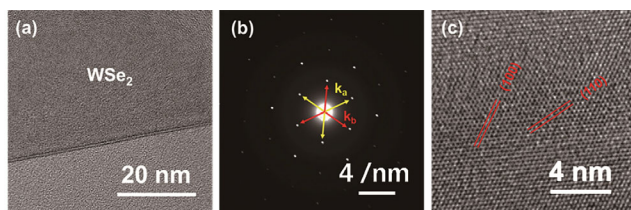


**Figure 4** (a) Low-magnification TEM image showing the straight edge of a WSe<sub>2</sub> flake. (b) Typical SAED pattern of the WSe<sub>2</sub> sample in (a). (c) High-magnification TEM image of the WSe<sub>2</sub> sample in (a) showing the uniform hexagonal lattice structure.

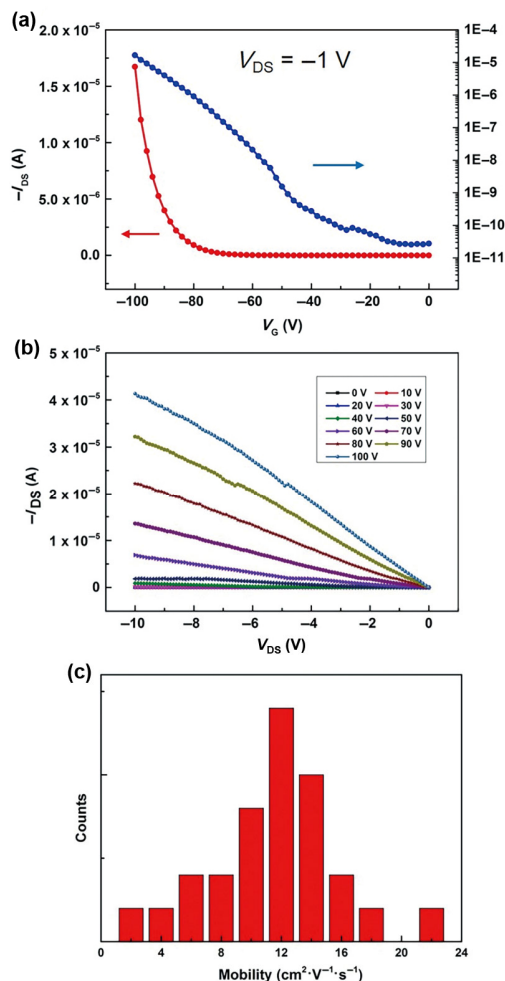


**Figure 5** Electrical characteristics of the back-gate FETs fabricated on continuous monolayer WSe<sub>2</sub> film. (a)  $I_{\text{DS}}-V_{\text{G}}$  and (b)  $I_{\text{DS}}-V_{\text{DS}}$  curves of a typical WSe<sub>2</sub> FET. (c) Histogram exhibiting the mobility distribution of 26 FETs fabricated on continuous monolayer WSe<sub>2</sub> film.

indicating that the WSe<sub>2</sub> grown by our gold-vapor-assisted CVD has a p-type behavior. In addition, the on current of the device was as high as  $1.7 \times 10^{-5}$  A and when a constant voltage of  $-1$  V was applied between the source and the drain, and the corresponding ON/OFF ratio is about  $6 \times 10^5$ . The field effect mobility of charge carriers can be calculated using the equation below

$$\mu = (dI_{\text{DS}}/dV_{\text{G}}) \times (L/(WC_{\text{i}}V_{\text{DS}}))$$

where  $L$  is the channel length,  $W$  is the channel width, and  $C_{\text{i}}$  is the gate oxide capacitance. In this way, the mobility extracted from the FET in Fig. 5(a) is around  $21 \text{ cm}^2\text{V}^{-1}\text{s}^{-1}$ . The  $I_{\text{DS}}-V_{\text{DS}}$  curves of the same device are plotted in Fig. 5(b). The linear output characteristic suggests that ohmic contacts were formed between the Ti/Au electrodes and the underneath WSe<sub>2</sub>. In order to investigate the quality of our WSe<sub>2</sub>, we measured 26 FETs fabricated by photolithography and plotted a histogram of mobility distribution in Fig. 5(c). The FETs showed decent mobility of  $12 \text{ cm}^2\text{V}^{-1}\text{s}^{-1}$  on average. The good FET performance demonstrates the uniformity of our continuous monolayer WSe<sub>2</sub> film formed by merging of aligned WSe<sub>2</sub> flakes, which is ready for potential large-scale nanofabrication processes.

## 4 Conclusion

In summary, we have successfully developed an Au-vapor-assisted CVD method to synthesize aligned monolayer WSe<sub>2</sub>. The advantages of this approach can be concluded as follows: (1) 97% of WSe<sub>2</sub> flakes in the downstream region have  $0^\circ$  and  $60^\circ$  edge orientations; (2) the edge size of the aligned monolayer WSe<sub>2</sub> flakes can be as large as  $130 \mu\text{m}$ ; (3) thanks to the catalytic effect of Au, our CVD set up can achieve a fast growth rate of  $4.3 \mu\text{m}\cdot\text{s}^{-1}$  and the growth time can be as short as 30 s. With Raman, PL, and TEM characterization and FET device study, we have demonstrated that the aligned monolayer WSe<sub>2</sub> performed good quality. The continuous monolayer WSe<sub>2</sub> film formed by individual aligned domains showed outstanding uniformity and electronic properties, and it is suitable for large-scale and low-cost nanofabrication processes like photolithography. We believe that the introduction of catalytic metal vapor should be able to impact the CVD process of other TMDCs with various substrates.

## Acknowledgements

We would like to acknowledge the collaboration of this research with King Abdul-Aziz City for Science and Technology (KACST) via The Center of Excellence for Nanotechnologies (CEGN). A portion of the images and data used in this article were generated at the Core Center of Excellence in Nano Imaging (CNI), University of Southern California.

**Electronic Supplementary Material:** Supplementary material (photograph of CVD growth setup, optical micrograph images of results of the control growth without Au foil, optical micrograph images of intermediate state of the formation of continuous monolayer WSe<sub>2</sub> film, optical micrograph images of devices on WSe<sub>2</sub> film, XPS measurements, EDX measurements) is available in the online version of this article at <https://doi.org/10.1007/s12274-020-2893-7>.

## References

- [1] Novoselov, K. S.; Mishchenko, A.; Carvalho, A.; Castro Neto, A. H. 2D materials and van der Waals heterostructures. *Science* **2016**, *353*,

- aac9439.
- [2] Xia, F. N.; Wang, H.; Xiao, D.; Dubey, M.; Ramasubramaniam, A. Two-dimensional material nanophotonics. *Nat. Photon.* **2014**, *8*, 899–907.
  - [3] Fang, H.; Chuang, S.; Chang, T. C.; Takei, K.; Takahashi, T.; Javey, A. High-performance single layered WSe<sub>2</sub> p-FETs with chemically doped contacts. *Nano Lett.* **2012**, *12*, 3788–3792.
  - [4] Liu, W.; Kang, J. H.; Sarkar, D.; Khatami, Y.; Jena, D.; Banerjee, K. Role of metal contacts in designing high-performance monolayer n-type WSe<sub>2</sub> field effect transistors. *Nano Lett.* **2013**, *13*, 1983–1990.
  - [5] Ma, Y. Q.; Liu, B. L.; Zhang, A. Y.; Chen, L.; Fathi, M.; Shen, C. F.; Abbas, A. N.; Ge, M. Y.; Mecklenburg, M.; Zhou, C. W. Reversible semiconducting-to-metallic phase transition in chemical vapor deposition grown monolayer WSe<sub>2</sub> and applications for devices. *ACS Nano* **2015**, *9*, 7383–7391.
  - [6] Liu, B. L.; Ma, Y. Q.; Zhang, A. Y.; Chen, L.; Abbas, A. N.; Liu, Y. H.; Shen, C. F.; Wan, H. C.; Zhou, C. W. High-performance WSe<sub>2</sub> field-effect transistors via controlled formation of in-plane heterojunctions. *ACS Nano* **2016**, *10*, 5153–5160.
  - [7] Sarkar, D.; Xie, X. J.; Kang, J. H.; Zhang, H. J.; Liu, W.; Navarrete, J.; Moskovits, M.; Banerjee, K. Functionalization of transition metal dichalcogenides with metallic nanoparticles: Implications for doping and gas-sensing. *Nano Lett.* **2015**, *15*, 2852–2862.
  - [8] Nam, H.; Oh, B. R.; Chen, M. K.; Wi, S. J.; Li, D.; Kurabayashi, K.; Liang, X. G. Fabrication and comparison of MoS<sub>2</sub> and WSe<sub>2</sub> field-effect transistor biosensors. *J. Vac. Sci. Technol. B* **2015**, *33*, 06FG01.
  - [9] Wu, F. Q.; Chen, L.; Zhang, A. Y.; Hong, Y. L.; Shih, N. Y.; Cho, S. Y.; Drake, G. A.; Fleetham, T.; Cong, S.; Cao, X. et al. High-performance sub-micrometer channel WSe<sub>2</sub> field-effect transistors prepared using a flood-dike printing method. *ACS Nano* **2017**, *11*, 12536–12546.
  - [10] Kelly, A. G.; Hallam, T.; Backes, C.; Harvey, A.; Esmaily, A. S.; Godwin, I.; Coelho, J.; Nicolosi, V.; Lauth, J.; Kulkarni, A. et al. All-printed thin-film transistors from networks of liquid-exfoliated nanosheets. *Science* **2017**, *356*, 69–73.
  - [11] Das, S.; Gulotty, R.; Sumant, A. V.; Roelofs, A. All two-dimensional, flexible, transparent, and thinnest thin film transistor. *Nano Lett.* **2014**, *14*, 2861–2866.
  - [12] Zheng, Z. Q.; Zhang, T. M.; Yao, J. D.; Zhang, Y.; Xu, J. R.; Yang, G. W. Flexible, transparent and ultra-broadband photodetector based on large-area WSe<sub>2</sub> film for wearable devices. *Nanotechnology* **2016**, *27*, 225501.
  - [13] Huang, J. K.; Pu, J.; Hsu, C. L.; Chiu, M. H.; Juang, Z. Y.; Chang, Y. H.; Chang, W. H.; Iwasa, Y.; Takenobu, T.; Li, L. J. Large-area synthesis of highly crystalline WSe<sub>2</sub> monolayers and device applications. *ACS Nano* **2014**, *8*, 923–930.
  - [14] Chen, J. Y.; Liu, B.; Liu, Y. P.; Tang, W.; Nai, C. T.; Li, L. J.; Zheng, J.; Gao, L. B.; Zheng, Y.; Shin, H. S. et al. Chemical vapor deposition of large-sized hexagonal WSe<sub>2</sub> crystals on dielectric substrates. *Adv. Mater.* **2015**, *27*, 6722–6727.
  - [15] Li, S. S.; Wang, S. F.; Tang, D. M.; Zhao, W. J.; Xu, H. L.; Chu, L. Q.; Bando, Y.; Golberg, D.; Eda, G. Halide-assisted atmospheric pressure growth of large WSe<sub>2</sub> and WS<sub>2</sub> monolayer crystals. *Appl. Mater. Today* **2015**, *1*, 60–66.
  - [16] Huang, J.; Yang, L.; Liu, D.; Chen, J.; Fu, Q.; Xiong, Y.; Lin, F.; Xiang, B. Large-area synthesis of monolayer WSe<sub>2</sub> on a SiO<sub>2</sub>/Si substrate and its device applications. *Nanoscale* **2015**, *7*, 4193–4198.
  - [17] Zhang, X. T.; Choudhury, T. H.; Chubarov, M.; Xiang, Y.; Jariwala, B.; Zhang, F.; Alem, N.; Wang, G. C.; Robinson, J. A.; Redwing, J. M. Diffusion-controlled epitaxy of large area coalesced WSe<sub>2</sub> monolayers on sapphire. *Nano Lett.* **2018**, *18*, 1049–1056.
  - [18] Yu, H.; Yang, Z. Z.; Du, L. J.; Zhang, J.; Shi, J.; Chen, W.; Chen, P.; Liao, M. Z.; Zhao, J.; Meng, J. L. et al. Precisely aligned monolayer MoS<sub>2</sub> epitaxially grown on h-BN basal plane. *Small* **2017**, *13*, 1603005.
  - [19] Chen, Z. X.; Liu, H. Q.; Chen, X. C.; Chu, G.; Chu, S.; Zhang, H. Wafer-size and single-crystal MoSe<sub>2</sub> atomically thin films grown on GaN substrate for light emission and harvesting. *ACS Appl. Mater. Interfaces* **2016**, *8*, 20267–20273.
  - [20] Ruzmetov, D.; Zhang, K. H.; Stan, G.; Kalanyan, B.; Bhimanapati, G. R.; Eichfeld, S. M.; Burke, R. A.; Shah, P. B.; O'Regan, T. P.; Crowne, F. J. et al. Vertical 2D/3D semiconductor heterostructures based on epitaxial molybdenum disulfide and gallium nitride. *ACS Nano* **2016**, *10*, 3580–3588.
  - [21] Ji, Q. Q.; Zhang, Y. F.; Gao, T.; Zhang, Y.; Ma, D. L.; Liu, M. X.; Chen, Y. B.; Qiao, X. F.; Tan, P. H.; Kan, M. et al. Epitaxial monolayer MoS<sub>2</sub> on mica with novel photoluminescence. *Nano Lett.* **2013**, *13*, 3870–3877.
  - [22] Ago, H.; Fukamachi, S.; Endo, H.; Solis-Fernandez, P.; Yunus, R. M.; Uchida, Y.; Panchal, V.; Kazakova, O.; Tsuji, M. Visualization of grain structure and boundaries of polycrystalline graphene and two-dimensional materials by epitaxial growth of transition metal dichalcogenides. *ACS Nano* **2016**, *10*, 3233–3240.
  - [23] Eichfeld, S. M.; Hossain, L.; Lin, Y. C.; Piasecki, A. F.; Kupp, B.; Birdwell, A. G.; Burke, R. A.; Lu, N.; Peng, X.; Li, J. et al. Highly scalable, atomically thin WSe<sub>2</sub> grown via metal–organic chemical vapor deposition. *ACS Nano* **2015**, *9*, 2080–2087.
  - [24] Ago, H.; Endo, H.; Solís-Fernández, P.; Takizawa, R.; Ohta, Y.; Fujita, Y.; Yamamoto, K.; Tsuji, M. Controlled van der Waals epitaxy of monolayer MoS<sub>2</sub> triangular domains on graphene. *ACS Appl. Mater. Interfaces* **2015**, *7*, 5265–5273.
  - [25] Lu, C. I.; Butler, C. J.; Huang, J. K.; Hsing, C. R.; Yang, H. H.; Chu, Y. H.; Luo, C. H.; Sun, Y. C.; Hsu, S. H.; Yang, K. H. O. et al. Graphite edge controlled registration of monolayer MoS<sub>2</sub> crystal orientation. *Appl. Phys. Lett.* **2015**, *106*, 181904.
  - [26] Dumcenco, D.; Ovchinnikov, D.; Marinov, K.; Lazić, P.; Gibertini, M.; Marzari, N.; Sanchez, O. L.; Kung, Y. C.; Krasnozhan, D.; Chen, M. W. Large-area epitaxial monolayer MoS<sub>2</sub>. *ACS Nano* **2015**, *9*, 4611–4620.
  - [27] Chen, L.; Liu, B. L.; Ge, M. Y.; Ma, Y. Q.; Abbas, A. N.; Zhou, C. W. Step-edge-guided nucleation and growth of aligned WSe<sub>2</sub> on sapphire via a layer-over-layer growth mode. *ACS Nano* **2015**, *9*, 8368–8375.
  - [28] Aljarb, A.; Cao, Z.; Tang, H. L.; Huang, J. K.; Li, M. L.; Hu, W. J.; Cavallo, L.; Li, L. J. Substrate lattice-guided seed formation controls the orientation of 2D transition-metal dichalcogenides. *ACS Nano* **2017**, *11*, 9215–9222.
  - [29] Ly, T. H.; Chiu, M. H.; Li, M. Y.; Zhao, J.; Perello, D. J.; Cichocka, M. O.; Oh, H. M.; Chae, S. H.; Jeong, H. Y.; Yao, F. et al. Observing grain boundaries in CVD-grown monolayer transition metal dichalcogenides. *ACS Nano* **2014**, *8*, 11401–11408.
  - [30] Tsvion, D.; Schwartzman, M.; Popovitz-Biro, R.; von Huth, P.; Joselevich, E. Guided growth of millimeter-long horizontal nanowires with controlled orientations. *Science* **2011**, *333*, 1003–1007.
  - [31] Kurnosikov, O.; Pham Van, L.; Cousty, J. About anisotropy of atomic-scale height step on (0001) sapphire surface. *Surf. Sci.* **2000**, *459*, 256–264.
  - [32] Heffelfinger, J. R.; Bench, M. W.; Carter, C. B. Steps and the structure of the (0001)  $\alpha$ -alumina surface. *Surf. Sci.* **1997**, *370*, L168–L172.
  - [33] Del Corro, E.; Terrones, H.; Elias, A.; Fantini, C.; Feng, S. M.; Nguyen, M. A.; Mallouk, T. E.; Terrones, M.; Pimenta, M. A. Excited excitonic states in 1L, 2L, 3L, and bulk WSe<sub>2</sub> observed by resonant Raman spectroscopy. *ACS Nano* **2014**, *8*, 9629–9635.
  - [34] Tonndorf, P.; Schmidt, R.; Böttger, P.; Zhang, X.; Börner, J.; Liebig, A.; Albrecht, M.; Kloc, C.; Gordan, O.; Zahn, D. R. T. et al. Photoluminescence emission and Raman response of monolayer MoS<sub>2</sub>, MoSe<sub>2</sub>, and WSe<sub>2</sub>. *Opt. Express* **2013**, *21*, 4908–4916.
  - [35] Xu, K.; Wang, Z. X.; Du, X. L.; Safdar, M.; Jiang, C.; He, J. Atomic-layer triangular WSe<sub>2</sub> sheets: Synthesis and layer-dependent photoluminescence property. *Nanotechnology* **2013**, *24*, 465705.
  - [36] Li, Y.; Hao, S. Q.; DiStefano, J. G.; Murthy, A. A.; Hanson, E. D.; Xu, Y. B.; Wolverson, C.; Chen, X. Q.; Dravid, V. P. Site-specific positioning and patterning of MoS<sub>2</sub> monolayers: The role of Au seeding. *ACS Nano* **2018**, *12*, 8970–8976.
  - [37] Song, I.; Park, C.; Hong, M. S.; Baik, J.; Shin, H. J.; Choi, H. C. Patternable large-scale molybdenum disulfide atomic layers grown by gold-assisted chemical vapor deposition. *Angew. Chem., Int. Ed.* **2014**, *53*, 1266–1269.
  - [38] Yun, S. J.; Chae, S. H.; Kim, H.; Park, J. C.; Park, J. H.; Han, G. H.; Lee, J. S.; Kim, S. M.; Oh, H. M.; Seok, J. et al. Synthesis of centimeter-scale monolayer tungsten disulfide film on gold foils. *ACS Nano* **2015**, *9*, 5510–5519.

- [39] Kim, H.; Song, I.; Park, C.; Son, M.; Hong, M.; Kim, Y.; Kim, J. S.; Shin, H. J.; Baik, J.; Choi, H. C. Copper-vapor-assisted chemical vapor deposition for high-quality and metal-free single-layer graphene on amorphous SiO<sub>2</sub> substrate. *ACS Nano* **2013**, *7*, 6575–6582.
- [40] Yang, C.; Wu, T. R.; Wang, H. M.; Zhang, X. F.; Shi, Z. Y.; Xie, X. M. Copper-vapor-catalyzed chemical vapor deposition of graphene on dielectric substrates. *Appl. Phys. Lett.* **2017**, *111*, 043107.
- [41] Teng, P. Y.; Lu, C. C.; Akiyama-Hasegawa, K.; Lin, Y. C.; Yeh, C. H.; Suenaga, K.; Chiu, P. W. Remote catalyzation for direct formation of graphene layers on oxides. *Nano Lett.* **2012**, *12*, 1379–1384.
- [42] Gao, Y.; Liu, Z. B.; Sun, D. M.; Huang, L.; Ma, L. P.; Yin, L. C.; Ma, T.; Zhang, Z. Y.; Ma, X. L.; Peng, L. M. et al. Large-area synthesis of high-quality and uniform monolayer WS<sub>2</sub> on reusable Au foils. *Nat. Commun.* **2015**, *6*, 8569.
- [43] Gao, Y.; Hong, Y. L.; Yin, L. C.; Wu, Z. T.; Yang, Z. Q.; Chen, M. L.; Liu, Z. B.; Ma, T.; Sun, D. M.; Ni, Z. H. et al. Ultrafast growth of high-quality monolayer WSe<sub>2</sub> on Au. *Adv. Mater.* **2017**, *29*, 1700990.
- [44] Liu, J. X.; Zeng, M. Q.; Wang, L. X.; Chen, Y. T.; Xing, Z.; Zhang, T.; Liu, Z.; Zuo, J. L.; Nan, F.; Mendes, R. G. et al. Ultrafast self-limited growth of strictly monolayer WSe<sub>2</sub> crystals. *Small* **2016**, *12*, 5741–5749.
- [45] Gurarlan, A.; Yu, Y. F.; Su, L. Q.; Yu, Y. L.; Suarez, F.; Yao, S. S.; Zhu, Y.; Ozturk, M.; Zhang, Y.; Cao, L. Y. Surface-energy-assisted perfect transfer of centimeter-scale monolayer and few-layer MoS<sub>2</sub> films onto arbitrary substrates. *ACS Nano* **2014**, *8*, 11522–11528.